Received 19 February 2024; revised 26 March 2024; accepted 28 March 2024. Date of publication 1 April 2024; date of current version 27 May 2024.

Digital Object Identifier 10.1109/OJAP.2024.3383791

A Compact Dual-Band Tripolarized Patch Antenna With Simple Structure and Very High Isolation

SON XUAT TA [1] (Senior Member, IEEE), TRAN HIEN BUI [1], KHAC KIEM NGUYEN [1] (Member, IEEE), AND NGHIA NGUYEN-TRONG [2] (Senior Member, IEEE)

[1]School of Electrical and Electronic Engineering, Hanoi University of Science and Technology, Hanoi 100000, Vietnam

[2]Nextwaves Industries, Ho Chi Minh 700000, Vietnam

CORRESPONDING AUTHOR: S. X. TA (e-mail: xuat.tason@hust.edu.vn)

This work was supported by the Vietnam National Foundation for Science and Technology Development (NAFOSTED) under Grant 102.04-2021.06.

ABSTRACT A compact dual-band tripolarized antenna with simple structure and high isolation operating at 2.45 GHz and 3.5 GHz bands is presented. The design is composed of a slotted patch and a monopolar patch connected together by four vias. The antenna uses a double differential-fed scheme for x- and y-horizontally polarized broadside radiations and a single-ended port at the center for vertically-polarized omnidirectional radiation. The combination of slotted patch, monopolar patch, and vias yields several interesting features, which are exploited in the design to achieve dual-band tripolarized operation. Thank to the differential feed scheme and structural symmetry, the proposed antenna achieves a very high isolation among all ports. For verification, the final design is fabricated and measured. The double differential-fed scheme are realized by using two wideband out-of-phase power dividers, whose operational bandwidth covers both 2.45 and 3.5 GHz bands. The antenna with profile of $0.09\lambda_{2.45-\text{GHz}}$ yields a measured 10-dB return loss bandwidth of $2.43 - 2.49$ GHz and $3.23 - 3.66$ GHz and isolation of ≥ 35 dB among all ports. Tripolarized radiation is verified with far-field measurement, showing highly symmetrical pattern and low cross-polarization in all three operational modes. The proposed design is a good candidate for dual-band communication systems which require polarization and pattern diversity antennas.

INDEX TERMS Compact size, dual-band operation, high isolation, monopolar, slotted patch, tripolarization.

I. INTRODUCTION

IN RICH-SCATTERING environment, the channel capacity can be significantly enhanced by employing an antenna system with three orthogonal polarizations, which is also named tripolarized antennas [1], [2], [3]. The interesting design problem of incorporating three orthogonal polarizations in a single device has motivated antenna researchers to create various innovative radiating structures in recent years. These antennas might be classified into four categories:

1) First is a class of 3-dimensional (3D) structures constructed by three orthogonal simple linear-polarized (LP) elements, for instant, half-wavelength dipoles [1], printed dipoles [4], slots [5], [6], [7], loops [8], and inverted-F antennas [9]. Most of these designs were initially used for the experimental validation of the tripolarized systems. Their main disadvantages are the narrow bandwidths and physical cubic configurations.
2) The second category includes modifications of a simple design in [2], which is composed of a two-port patch for dual-polarization in broadside and a $\lambda/4$-monopole for vertically LP omnidirectional radiation in the azimuth plane. The modifications were applied to both patch and monopole in order to improve the antenna performances [10], [11], [12], [13]; i.e., the dual-polarized patch is fed by proximity coupling instead of the probe feed in [2] to broaden bandwidth and enhance isolation, while the conventional monopole is replaced by top-loaded monopole to achieve a low-profile. With the coupling feed and top-loaded monopole, these designs require multi-layer structure.

Moreover, their bandwidths are constrained by the patch, which is normally narrow.

3) The third class utilizes multi-resonance modes of a same structure, including patches [14], [15], [16], [17], [18], [19], [20] and dielectric resonators [21]. While patches can support low profile designs, the dielectric resonator profile is typically higher. Nevertheless, all these designs suffer from a narrow bandwidth and low isolation.
4) The final category consists of designs with broad operational bandwidth and high isolation [22], [23], [24], [25], [26], [27], [28], [29], which are constructed by incorporating broadband vertically-polarized omni-directional elements and broadband dual-polarized antennas. The omnidirectional elements are such as driven-rod top-loaded monopole [22], monopolar patch [24], [25], [27], [29], printed monopole [26], and metasurface with shorting vias [28]. The broadband dual-polarized antennas are such as cross-slot-coupling patch [22], ring antenna [23], crossed dipoles [24], [25], [26], [27], metasurface [28], and slotted patch [29]. Their broadband and high-isolation features are, however, commonly accompanied with a complex configuration and large profile.

Generally, designing tripolarized antennas is a difficult task, especially when low profile and wide bandwidth are required. Furthermore, all aforementioned designs only operate in a single frequency band. Undoubtedly, achieving multi-band tripolarization is a critical challenge. Several dual-band multiport antennas have been reported, however, each port supports a distinct pattern in each single band [30], [31], [32], or one orthogonal polarization is missing [33], [34]. Up to now, there have been only two existing works reporting fully-functional dual-band tripolarized antenna [35], [36]. These designs, however, require multi-layered substrate, large footprint, and has quite limited bandwidth.

This paper proposes a low-profile dual-band tripolarized antenna for operation at 2.45 GHz and 3.5 GHz bands with simple structure, very high isolation, and enhanced impedance bandwidth. It is constructed by incorporating a slotted patch, a monopolar patch, and vias. Interestingly, this integration (when optimized) can enhance the performance of each individual radiating element. Furthermore, the design maintains a symmetrical structure, which theoretically provides an infinite isolation among all ports with differential feeding scheme.

II. ANTENNA DESIGN AND CHARACTERISTICS

A. ANTENNA GEOMETRY

The proposed antenna composes of a double-deferentially-fed patch for x- and y-polarized broadside radiations collocated with a monopolar patch for vertically polarized omnidirectional radiation (equivalent to a monopole in z-direction). For the dual-band operation, slotted and monopolar patches are incorporated with vias in this design, as illustrated in Fig. 1. The antenna is composed of a monopolar patch (Patch-2) with four vias, a slotted patch (Patch-1), four Γ-probes, two substrates (Sub. 1 and Sub. 2), and ground plane (GND). The substrates are Roger RT/Duroid 5880 sheets ($\varepsilon_r = 2.2$ and $\tan\delta = 0.0009$) with dimensions of 60 mm × 60 mm. Patch-1 is printed on the bottom side of Sub. 1, while the strips of Γ-probes are printed on the top side of Sub. 1. Patch 2 is printed on the top-side of Sub. 2. A slotted ring is inserted to the center of Patch-2 to improve the impedance matching, which is typical for monopolar patch antennas [15], [37]. The four metallic vias with diameter of $D = 1$ mm are passed through Sub. 1 and Sub. 2 to connect Patch-1 and Patch-2. The antenna is fed by five single ended ports (P_{1+}, P_{1-}, P_{2+}, P_{2-}, and P_3) via 50-Ω coaxial lines. Two pairs of P_{1+}/P_{1-} and P_{2+}/P_{2-} are for the horizontally-polarized broadside modes, while the P_3 is for the vertically-polarized omnidirectional mode. The outers of P_{1+}, P_{1-}, P_{2+}, and P_{2-} are connected to the GND, while their inners are passed through Sub. 1 to connect the strips of Γ-probes. For modeling the double differential-feed, in simulations, differential signals (i.e., same amplitude and phase-difference of 180°) are applied into the two pairs of P_{1+}/P_{1-} (P_{d1}) and P_{2+}/P_{2-} (P_{d2}). Different to other ports,

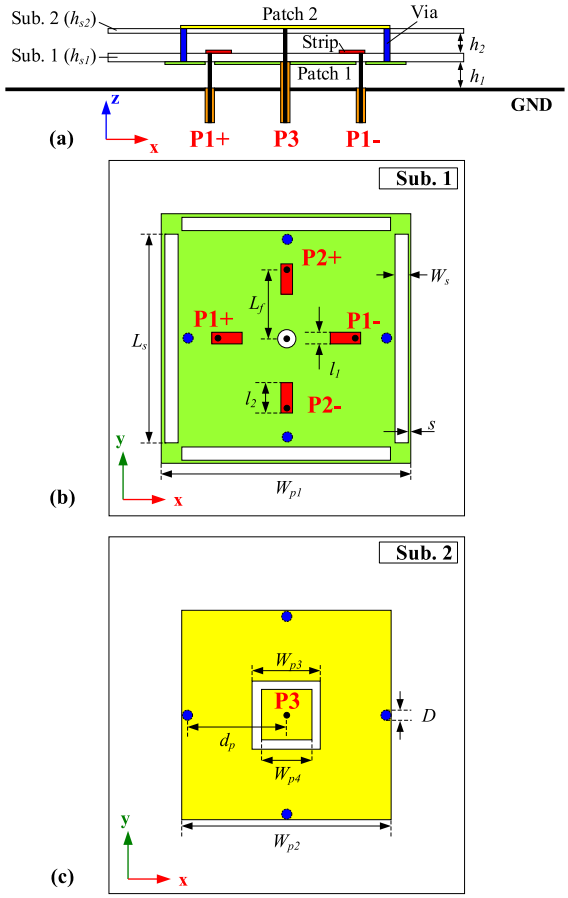

FIGURE 1. Geometry of the proposed antenna; (a) cross-sectional view, (b) top-view of Patch 1, (c) top-view of Patch 2. Note: the feeding network can be built using an additional substrate below the ground plane.

TABLE 1. Design parameters of the proposed antenna.

Par.	Value (mm)	Par.	Value (mm)	Par.	Value (mm)
h_{s1}	1.5748	h_{s2}	0.508	h_1	5
h_2	3	W_p	42	L_s	35.3
W_s	2.2	s	0.5	d_p	16.9
l_1	2.1	l_2	5	L_f	12
W_{p2}	34.8	W_{p3}	11.5	W_{p4}	8.4

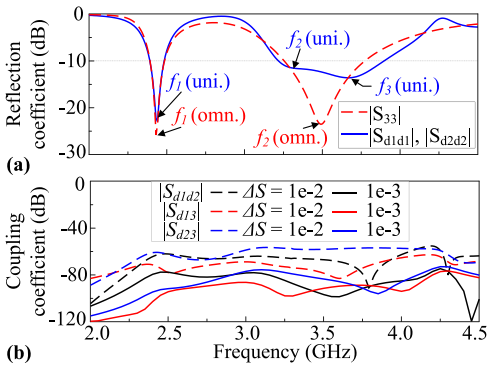

FIGURE 2. Simulated (a) reflection and (b) coupling coefficients of the proposed antenna.

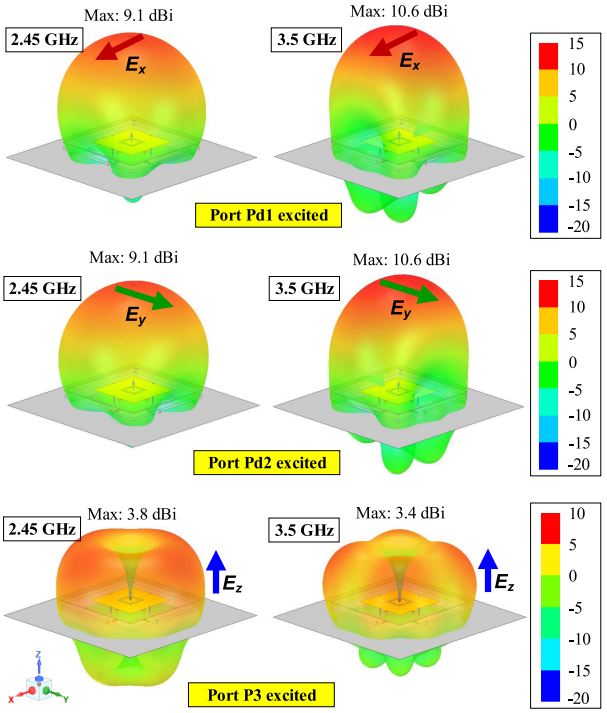

FIGURE 3. Simulated 3D radiation pattern of the proposed antenna for different excitation modes.

the coaxial line of P_3 passes through the GND, its outer is connected to Patch-1, while its inner passes through Sub. 1 and Sub. 2 to connect to Patch-2. The design parameters of the proposed antenna (optimized via ANSYS Electronics Desktop) are given in Table 1.

B. DUAL-BAND TRIPOLARIZED RADIATION

Fig. 2(a) shows the simulated reflection coefficients of the proposed antenna. The differential reflection coefficients (S_{d1d1} and S_{d2d2}) are calculated as in [38]:

$$S_{d1d1} = \frac{1}{2}(S_{1^+1^+} - S_{1^+1^-} - S_{1^-1^+} + S_{1^-1^-}) \quad (1)$$

$$S_{d2d2} = \frac{1}{2}(S_{2^+2^+} - S_{2^+2^-} - S_{2^-2^+} + S_{2^-2^-}) \quad (2)$$

It is observed that the overlapped bandwidth of all modes for reflection coefficient ≤ -10 dB are $2.39 - 2.48$ GHz (90 MHz) and $3.26 - 3.77$ GHz (510 MHz) for the lower and upper band, respectively. The radiation mechanisms for these modes will be further investigated in the next sub-sections.

The proposed antenna has 3 ports: two differential ports, i.e., P_{d1}, P_{d2}, and a single port in the middle P_3. Its port-to-port isolation can be derived as similarly as for a conventional differential-fed antennas [38]. The formula for isolation among three ports can be derived as follows:

$$S_{d1d2} = \frac{1}{2}(S_{1^+2^+} - S_{1^-2^-} - S_{1^-2^+} + S_{1^-2^-}) \quad (3)$$

$$S_{d_13} = \frac{1}{\sqrt{2}}(S_{1^+3} - S_{1^-3}) \quad (4)$$

$$S_{d_23} = \frac{1}{\sqrt{2}}(S_{2^+3} - S_{2^-3}) \quad (5)$$

The design in Fig. 1 exhibits double symmetry across (P_{1^+}, P_{1^-}), and (P_{2^+}, P_{2^-}). Furthermore, each pair of differential ports is also symmetrical across P_3. Thus, according to the equations (3), (4), and (5) all coupling between each pair of ports are zero ($S_{d1d2} = S_{d_13} = S_{d_23} = 0$).

In the full-wave simulation, when perfect symmetry is maintained, the couplings approach zero when the simulation errors go to zero. This is demonstrated in Fig. 2(b), which shows the simulated coupling coefficients of the antenna for different values of ΔS, i.e., error in S-parameters, in the ANSYS Electronics Desktop. For a meshing with $\Delta S = 0.01$, the simulated coupling coefficients are about -60 dB. When ΔS is decreased, the simulated coupling decreases towards its theoretical value of zero: with $\Delta S = 0.001$, the simulated coupling coefficients reach about -80 dB. The accuracy increment is accompanied by increasing computational time and computer resources. For the full-wave simulator, the computational time is dependent on the number of converged passes. With the same computer resources, the number of converged passes is 17 and 43 for $\Delta S = 0.01$ and 0.001, respectively.

To illustrate the tripolarized radiation, Fig. 3 shows the simulated 3D pattern of the proposed antenna for different excitation modes. It is observed that the antenna achieves a good tripolarized radiation at both frequency-bands. For the broadside modes, the simulations result in a gain of 9.1 dBi and 10.6 dBi at 2.45 GHz and 3.5 GHz, respectively. For the monopolar mode, the antenna yields a conical radiation

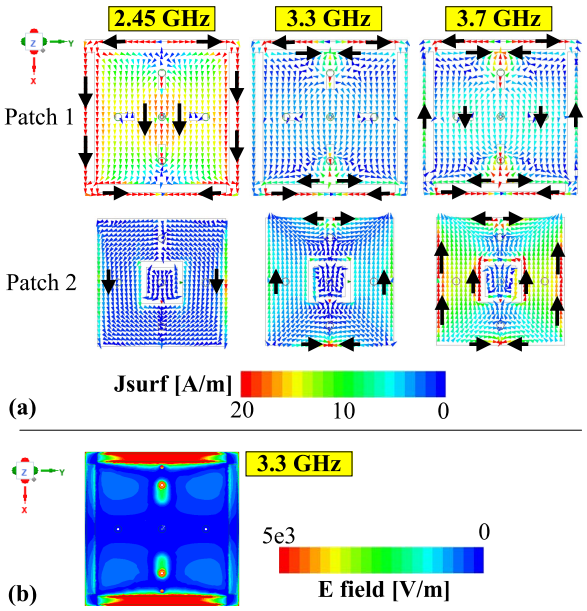

FIGURE 4. (a) Current distributions on the proposed antennas at the three resonances and (b) E-files on Patch 1 at 3.3 GHz when the P_{d1} is excited and other ports are terminated by 50-Ω loads.

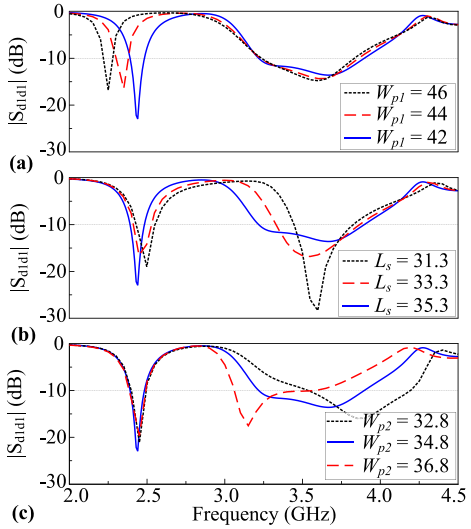

FIGURE 5. Simulated $|S_{d1d1}|$ of the proposed antenna for different values of the key parameters: (a) width of Patch 1 (W_{p1}), (b) slot length (L_s), and (c) width of Patch 2 (W_{p2}). (unit: mm).

pattern with gain of 3.8 dBi and 3.4 dBi at the lower and upper frequencies, respectively.

C. DUAL-POLARIZED BROADSIDE RADIATION MODES

As shown in Fig. 2(a), the combination of slotted and monopolar patches yields three resonances in the $|S_{d1d1}|$ curve, i.e., at 2.45, 3.3, and 3.7 GHz. Although dual-band slotted patch was proposed in [39], it exhibited narrow bandwidth in both bands. Meanwhile, the proposed design (Fig. 1) is able to cover a much wider bandwidth in the upper band which is valuable such as for the sub-6 GHz 5G applications.

The three resonances in an integrated structure are interesting and their physical reasons should be discussed. First, the current distributions on the two patches for different resonances of the broadside modes are plotted in Fig. 4(a). At 2.45 GHz, dominant currents show the fundamental TM 10 mode on Patch-1. The strong currents at 3.3 GHz are mostly around the slots of Patch-1, while the dominant currents at 3.7 GHz are mostly concentrated on Patch-2 only, also with TM 10 mode. To confirm the slot mode at 3.3 GHz, the E-fields on Patch-1 are simulated at 3.3 GHz and given in Fig. 4(b). It is clear that the E-fields mainly occupy on the slots. Based on Fig. 4, we can conclude that the Patch-2 generates the third resonance which is merged with the slot mode of Patch-1 to broaden the upper band. Thus, the integration of the monopolar patch, i.e., Patch-2, does not only provide the third mode (omnidirectional) but also improves the performance of the broadside modes.

To confirm the above observations, a parametric study is carried out for several key parameters and given in Fig. 5. This study confirms that (i) the lower band is mainly determined by W_{p1}; (ii) the upper band mainly depends on L_s and W_{p2}.

D. VERTICALLY-POLARIZED OMNIDIRECTIONAL RADIATION MODE

As shown in Fig. 2(a), the proposed antenna yields two distinct resonances at 2.45 and 3.5 GHz in the $|S_{33}|$ curve. It should be noted that a conventional monopolar patch antenna only yields a single resonance band, e.g., [15]. Thus, the sources of these two resonances are analyzed as follows.

First, the current distribution are simulated at the two resonances as illustrated in the left side of Fig. 6. At 2.45 GHz, strong currents are distributed across the whole structure. At 3.5 GHz, the current distribution is mostly around the slots of Patch-1. To clearly see the slot mode at 3.5 GHz, the E-field distributions on the antenna are simulated when P_3 is excited (right side of Fig. 6). At 3.5 GHz, the field mainly occupy on the slots of Patch-1. These results indicate that the lower resonance caused by the entire structure, while the upper one belongs to the slot mode of Patch-1. The four slots have the same resonance frequency as in the broadside mode, however, they are radiating with the same phase, giving an equivalent magnetic current loop, and thus a monopolar pattern is achieved. Again, this is an interesting feature which is not seen in a single monopolar patch design.

A key parametric study is carried out for the omnidirectional radiation mode and given in Fig. 7. It is observed that the lower resonance is affected by all three parameters, including width of Patch-1 (W_{p1}), slot length (L_s), and width of Patch-2 (W_{p2}), whereas the upper resonance is mainly determined by L_s. Since Patch 1 is connected to Patch 2 by four vias, W_{p2} also controls the upper resonance. In summary, Figs. 5 and 7 can serve as a guideline for the optimization process.

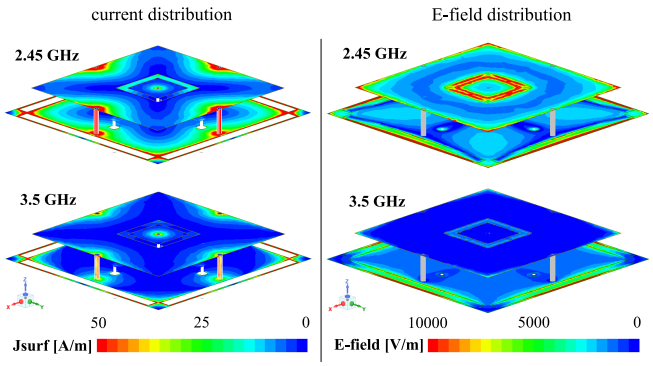

FIGURE 6. Current distributions and E-fields on the proposed antennas at 2.45 and 3.5 GHz when P_3 is excited and other ports are terminated by 50-Ω loads.

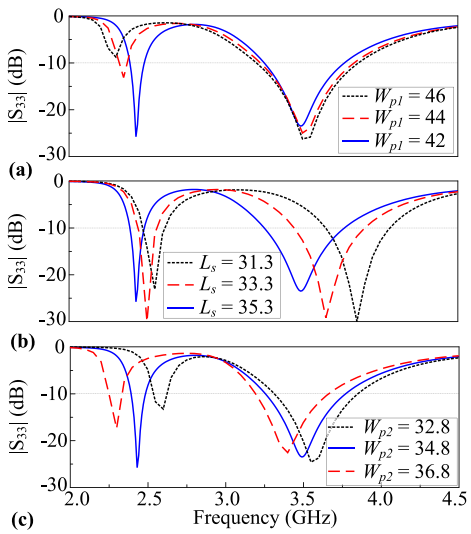

FIGURE 7. Simulated $|S_{33}|$ of the proposed antenna for different values of the key parameters: (a) width of Patch 1 (W_{p1}), (b) slot length (L_s), and (c) width of Patch 2 (W_{p2}). (unit: mm).

E. EFFECTS OF VIAS CONNECTING PATCH 1 AND PATCH 2

The dual-band tripolarization of the proposed antenna is obtained by incorporating the slotted and monopolar patches, and shorting vias. Accordingly, the antenna features are significantly affected by the vias connecting Patch 1 and Patch 2. To investigate these effects, the proposed antenna is characterized for different via diameters (D) and its results are given in Fig. 8. For the broadside modes, the presence of vias merges the second and third resonances in the S_{d1d1} (S_{d2d2}) curves, and consequently, broaden the upper band, as shown in Fig. 8(a). Also, it is observed that the via diameter hardly affects the broadside radiation modes.

For the vertically polarized omnidirectional mode, as shown in Fig. 8(b), without vias, Patch 1 is separated to Patch 2, thereby the antenna yields only one resonance at 3 GHz in the S_{33} curve. Due to the presence of vias, the antenna achieves two resonances which are significantly affected by the via diameter (D). As D increased, both lower and upper resonances shifted toward the higher frequencies.

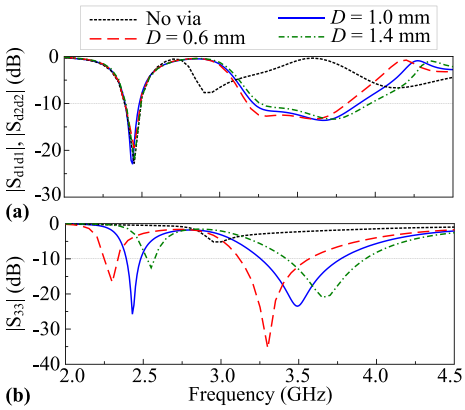

FIGURE 8. Simulated (a) S_{d1d1}, S_{d2d2} and (b) $|S_{33}|$ values of the proposed antenna for different diameters (D) of vias connecting Patch 1 and Patch 2.

These effects are similar to the conventional monopolar patch antenna [40]. As explained in [40], when the diameter of via increases, the resonant current path decreases, and therefore, the resonance frequencies increase. From Fig. 8(b), the $D =$ 1.0 mm offers two resonances at the desired frequencies of 2.45 and 3.5 GHz.

III. REALIZATION AND MEASUREMENTS

A. REALIZATION OF DIFFERENTIAL FEED

To realize the differential feed, out-of-phase power divider (PD) is needed. In this work, two wideband out-of-phase power dividers (PDs) are employed for the double differential-fed scheme of the proposed dual-band tripolarized antenna. Fig. 9(a) shows transmission-line schematic of the out-of-phase PD, which consists of a Wilkinson PD and a wideband 180° phase shifter. This design is a modification of planar balun in [41] where the conventional phase-delay line is replaced by a 90° Schiffman phase shifter with two-section stepped-impedance coupled line [42] to broaden the operational bandwidth. The out-of-phase PD is deployed on Roger RO4003 substrate ($\varepsilon_r = 3.38$, $\tan\delta = 0.0027$, and thickness of 0.8128 mm) and optimized for a bandwidth covering both 2.45 and 3.5 GHz bands.

The simulated S-parameters and phase-difference at outputs of the PD are given in Fig. 9(b). The reflection coefficient ($|S_{11}|$) at the input and coupling coefficient ($|S_{32}|$) between two output ports are ≤ -10 dB across the examined frequency range of 2.0 − 4.5 GHz. At 2.2 − 3.8 GHz, the phase and amplitude-differences between the output ports are $180 \pm 3°$ and ± 0.3 dB, respectively.

B. MEASUREMENTS

The dual-band tripolarized antenna was fabricated and measured. A fabricated prototype with overall size of 110 mm × 110 mm × 10.9 mm is shown in Fig. 10. Its components including monopolar patch, slotted patch, and feeding network are realized by using the printed circuit board technology. All components are fasted together by using plastic post and screw to construct the final prototype.

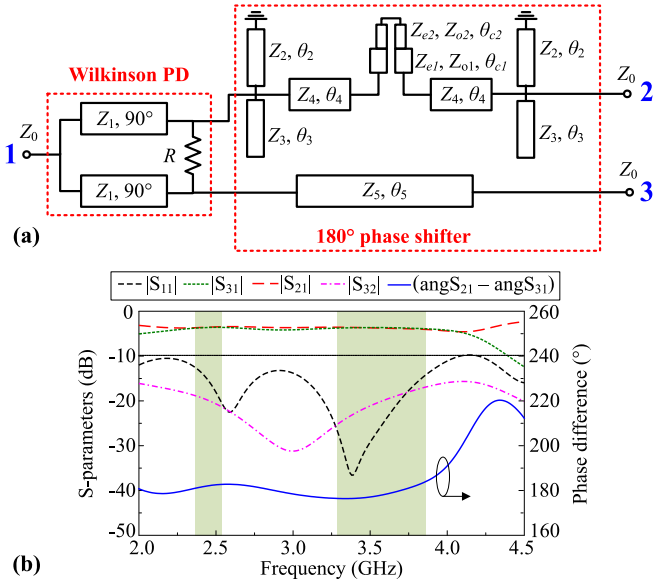

FIGURE 9. (a) Transmission-line schematic of wideband out-of-phase PD (its optimized parameters at 3-GHz: $Z_0 = 50\ \Omega$, $Z_1 = 70.7\ \Omega$, $R = 100\ \Omega$, $Z_2 = 61.8\ \Omega$, $\theta_2 = 51.9°$, $Z_3 = 63.5\ \Omega$, $\theta_3 = 45.9°$, $Z_4 = 50\ \Omega$, $\theta_4 = 53.6°$, $Z_5 = 50\ \Omega$, $\theta_5 = 485.4°$, $Z_{e1} = 51.1\ \Omega$, $Z_{o1} = 32\ \Omega$, $\theta_{c1} = 55.1°$, $Z_{e2} = 81.2\ \Omega$, $Z_{o2} = 43.6\ \Omega$, $\theta_{c2} = 39.3°$) and (b) its simulated S-parameters and phase difference at the outputs.

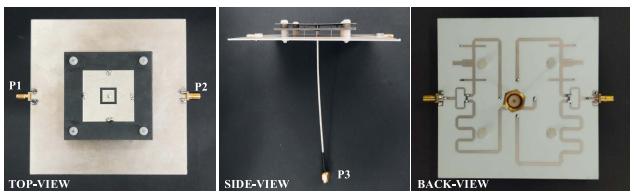

FIGURE 10. Fabricated sample of the dual-band tripolarized antenna.

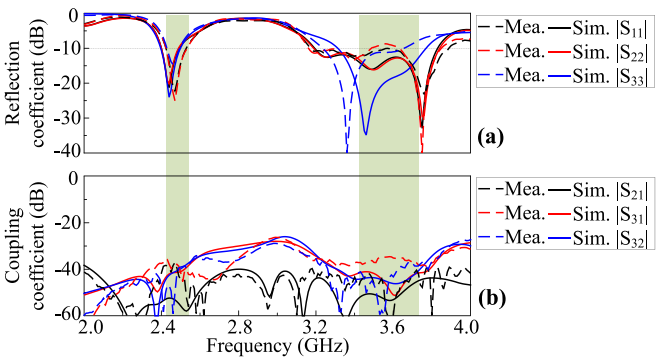

FIGURE 11. Measurement and simulation (a) reflection and (b) coupling coefficients of the antenna prototype.

The double differential-fed scheme is realized by using the two wideband out-of-phase PDs, while a RG405 semi-rigid coaxial cable is directly used for the P_3. Two SMA connectors are utilized at the inputs of feeding network (i.e., P1 and P2), which act as coaxial-to-microstrip line transitions.

The S-parameters of the fabricated prototype are measured by using three ports of Keysight N5244A PNA-X network analyzers and compared with the simulated results in Fig. 11.

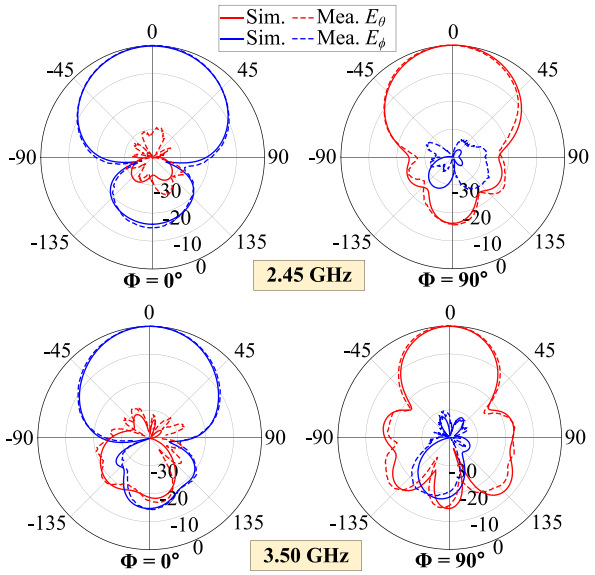

FIGURE 12. The normalized radiation pattern of the antenna prototype when P_1 excited (other ports are terminated by 50-Ω loads).

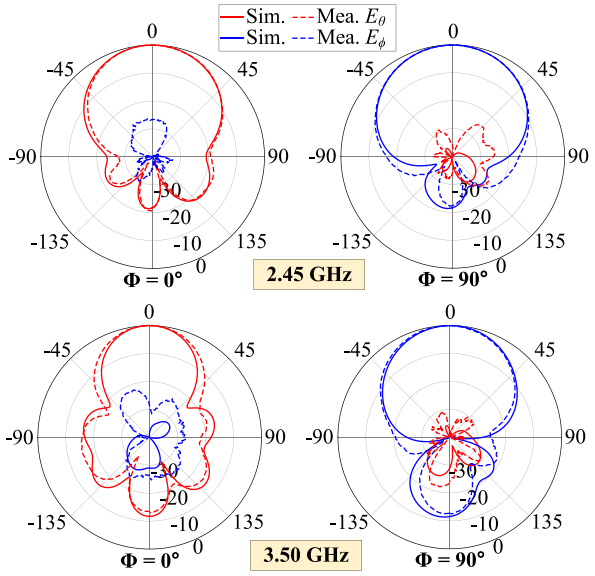

FIGURE 13. The normalized radiation pattern of the antenna prototype when P_2 excited (other ports are terminated by 50-Ω loads).

The results confirm that the antenna operates with dual-band characteristics in all radiation modes and low coupling coefficients. The measurements result in an overlapped bandwidth of 2.43 – 2.49 GHz and 3.23 – 3.66 GHz for all $|S_{ii}|$ <–10 dB ($i = 1, 2, 3$). Within the overlapped bandwidth, the measured coupling coefficients are < –35 dB, while the simulated values are < –40 dB. Very minor breach occurs in $|S_{22}|$ at about 3.6 GHz (about −9 dB). A slight discrepancy between the simulation and measurement is attributed to the fabrication tolerances.

Figs. 12, 13, and 14 plot the normalized radiation patterns of the antenna when P_1–P_3 are excited, respectively.

TABLE 2. Comparison of the proposed design with the previous dual-band multiport antennas.

Ant.	Category	No. of port	Feeding technique	Overall size (λ_L)	Structure	Frequency (GHz)	Bandwidth (%)	Iso. (dB)	Peak gain (dBi) at different ports for lower/upper bands
[30]	Each port for single band	2	Single-ended	$\pi\times0.44^2\times0.013$	1 substrate	2.40/ 5.80	3.54/ 3.45	26	0.75 (omni-) / 5.4 (uni-)
[31]	Each port for single band	2	Single-ended	$0.4\times0.4\times0.02$	2 substrates	2.45/ 5.80	8.16/ 10.34	18	2.0 (omni-) / 11.0 (uni-)
[32]	Each port for single band	3	Differential	$0.74\times0.74\times0.03$	2 substrates	2.45/ 5.80	6.53/ 6.90	30	3.4 (omni-) / 8.5 (uni-)
[33]	Each port for two bands	2	Single-ended	$0.88\times0.88\times0.06$	2 substrates	2.40/ 3.50	7.67/ 4.46	22.3	9.8 (uni-), 5.8 (omni-) / 7.1 (uni), 4.5 (omni-)
[34]	Each port for two bands	2	Single-ended	$1.0\times0.83\times0.12$	2 substrates	2.50/ 5.98	14.72/ 17.0	20	8.6 (uni-), 4.0 (omni-) / 4.5 (uni-), 5.6 (omni-)
[39]	Each port for two bands	2	Differential	$0.9\times0.9\times0.06$	2 substrates	2.45/ 5.20	4.90/ 6.15	41	8.5 (uni-), 8.5 (uni-) / 9.2 (uni-), 9.2 (uni-)
[35]	Each port for two bands	3	Single-ended	$\pi\times0.39^2\times0.07$	8 substrates	2.40/ 5.80	1.46/ 1.47	15	6.8 (uni-), 6.7 (uni-), 2.3 (omni-) / 9.0 (uni-), 9.2 (uni-), 6.6 (omni-)
[36]	Each port for two bands	3	Differential	$\pi\times0.49^2\times0.07$	4 substrates	2.45/ 5.80	2.04/ 3.10	40	7.1 (uni-), 7.1 (uni-), 4.1 (omni-) / 6.6 (uni-), 6.6 (uni-), 7.2 (omni-)
Pro.	Each port for two bands	3	Differential	$0.9\times0.9\times0.09$	3 substrates	2.45/ 3.50	2.45/ 12.30	35	8.9 (uni-), 8.9 (uni-), 4.6 (omni-) / 10.9 (uni-), 10.9 (uni-), 4.2 (omni-)

λ_L is the free space wavelength referring to the lower frequency.

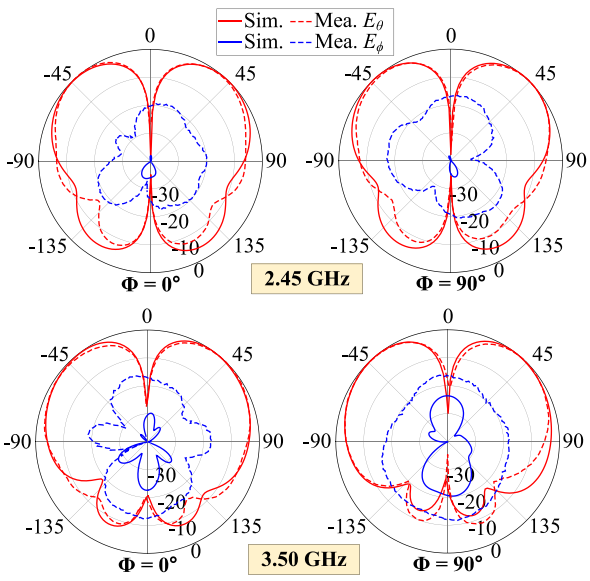

FIGURE 14. The normalized radiation pattern of the antenna prototype when P_3 excited (other ports are terminated by 50-Ω loads).

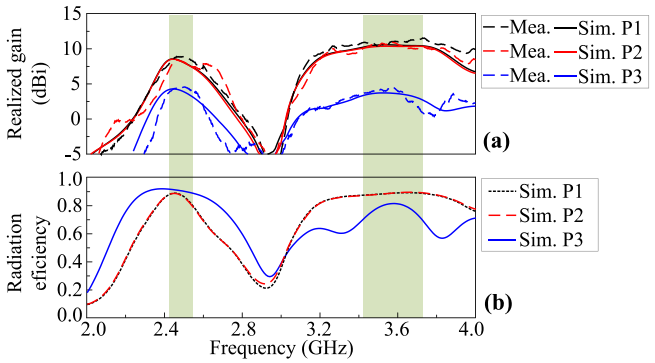

FIGURE 15. (a) Measured and simulated realized gains and (b) simulated radiation efficiencies of the antenna prototype at three ports.

The measured results agreed well with the computational predictions. It is observed that the antenna achieves excellent tripolarized radiation at dual bands. For the broadside modes, the measurements result in a cross-polarization level of ≤ -25 dB and front-to-back (FTB) ratio of ≥ 13 dB at both bands. Higher FTB can be obtained simply by extending the ground plane and shielding the feeding network. For the omnidirectional mode, the measurements result in the maximum gain in $\theta = 45°$ plane at both bands. Also, at the $\theta = 45°$ directions, the cross-polarization levels are -20 dB, which is higher than the simulated values. This discrepancy is due to the limitation of our anechoic chamber when measuring monopolar patterns.

Fig. 15(a) illustrates the realized gains of the antenna prototype. For P_1/P_2 excitation, the measured broadside gains are $7.2-8.9$ dBi and $9.3-10.9$ dBi at the lower and upper bands, respectively, whereas the simulated values are $8.0-8.5$ dBi and $9.4-10.5$ dBi. For P_3 excitation, the measured peak gains are $4.0-4.6$ dBi and $2.0-4.2$ dBi at the lower and upper bands, respectively, which are similar to the simulated values of $3.9-4.3$ dBi and $2.2-3.5$ dBi.

The simulated radiation efficiencies of the proposed antenna are illustrated in Fig. 15(b). Due to the limit function of the chamber, the efficiency of the antenna is not available. Nevertheless, since the measured gain is very close to the simulated gain, the simulated efficiency should give a reasonable prediction on the efficiency of the prototype. For the broadside radiations, although the efficiency is affected by the losses of feeding network, the design still achieves an efficiency value of $\geq 80\%$ at both operational bands. For the omnidirectional radiation, the prototype achieves peak values of 91% and 81% at the lower and upper bands, respectively.

C. COMPARISON AND DISCUSSION

Finally, a comprehensive comparison between the proposed design and the previous dual-band multiport antennas is given in Table 2. Most of the priors do not obtain fully-functional dual-band tripolarization. In the dual-band dual-mode antennas [30], [31], [32], each port is for either lower or upper band only. In [33], [34], [39], one orthogonal polarization is missing. As compared to the existing dual-band tripolarized antennas [35], [36], the proposed prototype used the least number of layers with a simpler configuration and easy realization while keeping a low-profile structure. Relative to the priors, the proposed prototype achieves a significantly broader bandwidth, higher gain, and more stable pattern. Moreover, our antenna size is reported with full GND, which could be made smaller with a more compact feeding network, e.g., with higher-permittivity substrate.

IV. CONCLUSION

We have presented a tripolarized antenna with dual-band operation at 2.45 and 3.5 GHz. The integration of a slotted patch, a monopolar patch, and connecting vias yields improvements for all radiation modes, which leads to two distinct operational bands with the upper-band bandwdith broadened. Due to the structural symmetry and differential feeding, zero coupling coefficients among all ports can be obtained theoretically. For realization, two wideband out-of-phase power dividers are employed as the double differential feeding network. The antenna achieved an excellent dual-band tripolarized radiation with symmetrical pattern and low cross-polarization. Many features, including simple configuration, compact-size, dual-band, tripolarization, high isolation, make the proposed antenna being a good candidate for the indoor environments of the 5G, WiMAX, as well as WLAN systems.

REFERENCES

[1] M. R. Andrews, P. P. Mitra, and R. de Carvalho, "Tripling the capacity of wireless communications using electromagnetic polarization," *Nature*, vol. 409, pp. 316–318, Jan. 2001.

[2] N. K. Das, T. Inoue, T. Taniguchi, and Y. Karasawa, "An experiment on MIMO system having three orthogonal polarization diversity branches in multipath-rich environment," in *Proc. IEEE Veh. Technol. Conf.*, vol. 2, 2004, pp. 1528–1532.

[3] M. C. Mtumbuka and D. J. Edwards, "Investigation of tri-polarised MIMO technique," *Electron. Lett.*, vol. 41, no. 3, pp. 137– 138, Feb. 2005.

[4] C. Chiu, J. Yan, and R. D. Murch, "Compact three-port orthogonally polarized MIMO antennas," *IEEE Antennas Wireless Propag. Lett.*, vol. 6, pp. 619–622, 2007.

[5] J. Sarrazin, Y. Mahe, S. Avrillon, and S. Toutain, "Investigation on cavity/slot antennas for diversity and MIMO systems: The example of a three-port antenna," *IEEE Antennas Wireless Propag. Lett.*, vol. 7, pp. 414–417, 2008.

[6] K. Tong, H. Tang, A. Al-Armaghany, and W. Hong, "Low-profile orthogonally tripolarized antennas," *IEEE Antennas Wireless Propag. Lett.*, vol. 12, pp. 876–879, 2013.

[7] L. Liu, C. Liu, Z. Li, X. Yin, and Z. N. Chen, "Slit-slot line and its application to low cross-polarization slot antenna and mutual-coupling suppressed tripolarized MIMO antenna," *IEEE Trans. Antennas Propag.*, vol. 67, no. 1, pp. 4–15, Jan. 2019.

[8] D. Piao, L. Yang, Q. Guo, Y. Mao, and Z. Li, "Measurement-based performance comparison of colocated tripolarized loop and dipole antennas," *IEEE Trans. Antennas Propag.*, vol. 63, no. 8, pp. 3371–3379, Aug. 2015.

[9] C. Chiu, J. Yan, R. D. Murch, J. X. Yun, and R. G. Vaughan, "Design and implementation of a compact 6-port antenna," *IEEE Antennas Wireless Propag. Lett.*, vol. 8, pp. 767–770, 2009.

[10] H. Zhong, Z. Zhang, W. Chen, Z. Feng, and M. F. Iskander, "A tripolarization antenna fed by proximity coupling and probe," *IEEE Antennas Wireless Propag. Lett.*, vol. 8, pp. 465–467, 2009.

[11] X. Gao, H. Zhong, Z. Zhang, Z. Feng, and M. F. Iskander, "Low-profile planar tripolarization antenna for WLAN communications," *IEEE Antennas Wireless Propag. Lett.*, vol. 9, pp. 83–86, 2010.

[12] J. Zheng, X. Gao, Z. Zhang, and Z. Feng, "A compact eighteen-port antenna cube for MIMO systems," *IEEE Trans. Antennas Propag.*, vol. 60, no. 2, pp. 445–455, Feb. 2012.

[13] Y. Yao, J. Zheng, and Z. Feng, "Diversity measurements for on-body channels using a tri-polarization antenna at 2.45 GHz," *IEEE Antennas Wireless Propag. Lett.*, vol. 11, pp. 1285–1288, 2012.

[14] S. Yan and G. A. E. Vandenbosch, "Wearable antenna with tripolarisation diversity for WBAN communications," *Electron. Lett.*, vol. 52, no. 7, pp. 500–502, 2016.

[15] N. P. Lawrence, C. Fumeaux, and D. Abbott, "Planar triorthogonal diversity slot antenna," *IEEE Trans. Antennas Propag.*, vol. 65, no. 3, pp. 1416–1421, Mar. 2017.

[16] D. Piao and Y. Wang, "Tripolarized MIMO antenna using a compact single-layer microstrip patch," *IEEE Trans. Antennas Propag.*, vol. 67, no. 3, pp. 1937–1940, Mar. 2019.

[17] D. Piao and Y. Wang, "Experimental evaluation of the tri-polarized MIMO channel properties based on a compact multimode antenna," *IEEE Access*, vol. 7, pp. 67807–67817, 2019.

[18] K. Zhang, Z. H. Jiang, W. Hong, and D. H. Werner, "A low-profile and wideband triple-mode antenna for wireless body area network concurrent on-/off-body communications," *IEEE Trans. Antennas Propag.*, vol. 68, no. 3, pp. 1982–1994, Mar. 2020.

[19] D. Piao, M. Wang, J. Zuo, L. Zhang, and Y. Wang, "Compact and low-coupled tripolarized microstrip MIMO antenna based on parasitic patch loading," *IEEE Trans. Antennas Propag.*, vol. 69, no. 9, pp. 5992–5997, Sep. 2021.

[20] Y. Wang, D. Piao, and J. Zuo, "A wide-angle and fully polarimetric retrodirective array based on tri-polarized antennas with pattern complementation," *IEEE Trans. Antennas Propag.*, vol. 70, no. 6, pp. 4518–4525, Jun. 2022.

[21] X. S. Fang, K. W. Leung, and K. M. Luk, "Theory and experiment of three-port Polarization-diversity cylindrical dielectric resonator antenna," *IEEE Trans. Antennas Propag.*, vol. 62, no. 10, pp. 4945–4951, Oct. 2014.

[22] Y. Zhang, K. Wei, Z. Zhang, and Z. Feng, "A broadband patch antenna with tripolarization using quasi-cross-slot and capacitive coupling feed," *IEEE Antennas Wireless Propag. Lett.*, vol. 12, pp. 832–835, 2013.

[23] K. Saurav, N. K. Mallat, and Y. M. M. Antar, "A three-port polarization and pattern diversity ring antenna," *IEEE Antennas Wireless Propag. Lett.*, vol. 17, no. 7, pp. 1324–1328, Jul. 2018.

[24] N. Nguyen-Trong, S. X. Ta, M. Ikram, K. Bertling, and A. M. Abbosh, "A low-profile wideband tripolarized antenna," *IEEE Trans. Antennas Propag.*, vol. 67, no. 3, pp. 1946–1951, Mar. 2019.

[25] S. X. Ta, D. Nguyen-Thi, K. K. Nguyen, C. Dao-Ngoc, and N. Nguyen-Trong, "Design of a low-profile tripolarized antenna with wide bandwidth," *IEEE Access*, vol. 7, pp. 82701–82708, 2019.
[26] S. X. Ta, D. M. Nguyen, K. K. Nguyen, C. Dao-Ngoc, and N. Nguyen-Trong, "A tripolarized antenna with ultrawide operational bandwidth," *IEEE Trans. Antennas Propag.*, vol. 68, no. 6, pp. 4386–4396, Jun. 2020.
[27] B. Feng, J. Chen, S. Yin, C.-Y.-D. Sim, and Z. Zhao, "A tripolarized antenna with diverse radiation characteristics for 5G and V2X communications," *IEEE Trans. Veh. Technol.*, vol. 69, no. 9, pp. 10115–10126, Sep. 2020.
[28] Z. Wang, S. Liu, and Y. Dong, "Low-profile metasurface-based antenna with tripolarization for 5G applications," *IEEE Trans. Antennas Propag.*, vol. 69, no. 9, pp. 5437–5445, Sep. 2021.
[29] L. Y. Nie, B. K. Lau, H. Aliakbari, S. Xiang, B. Wang, and X. Q. Lin, "A low-profile wideband dual-resonance tri-port MIMO antenna," *IEEE Trans. Antennas Propag.*, vol. 70, no. 6, pp. 4866–4871, Jun. 2022.
[30] Z. G. Liu and Y. X. Guo, "Dual band low profile antenna for body centric communications," *IEEE Trans. Antennas Propag.*, vol. 61, no. 4, pp. 2282–2285, Apr. 2013.
[31] C.-X. Mao, D. H. Werner, Y. Zhang, and X.-Y. Zhang, "Compact dual-band dual-mode antenna with Omni-/unidirectional radiation characteristics," *IEEE Antennas Wireless Propag. Lett.*, vol. 18, pp. 2657–2660, 2019.
[32] T. H. Bui, S. X. Ta, K. K. Nguyen, C. Dao-Ngoc, and N. Nguyen-Trong, "Planar high-isolation dual-band dual-mode antenna with omni-/unidirectional radiation," *IEEE Antennas Wireless Propag. Lett.*, vol. 21, pp. 99–103, 2022.
[33] S. Yan and G. A. E. Vandenbosch, "Low-profile dual-band pattern diversity patch antenna based on composite right/left-handed transmission line," *IEEE Trans. Antennas Propag.*, vol. 65, no. 6, pp. 2808–2815, Jun. 2017.
[34] X. Liu, Y. Wu, Z. Zhuang, W. Wang, and Y. Liu, "A dual-band patch antenna for pattern diversity application," *IEEE Access*, vol. 6, pp. 51986–51993, 2018.
[35] K. Zhang, Z. H. Jiang, T. Yue, Y. Zhang, W. Hong, and D. H. Werner, "A compact dual-band triple-mode antenna with pattern and Polarization diversities enabled by shielded mushroom structures," *IEEE Trans. Antennas Propag.*, vol. 69, no. 10, pp. 6229–6243, Oct. 2021.
[36] S. X. Ta, T. T. Phung, K. K. Nguyen, and N. Nguyen-Trong, "Low-profile dual-band tripolarized antenna using monopolar slotted patch," *IEEE Antennas Wireless Propag. Lett.*, vol. 22, no. 12, pp. 2925–2929, Dec. 2023.
[37] N. Nguyen-Trong, A. Piotrowski, and C. Fumeaux, "A frequency-reconfigurable dual-band low-profile monopolar antenna," *IEEE Trans. Antennas Propag.*, vol. 65, no. 7, pp. 3336–3343, Jul. 2017.
[38] B. R. Eisenstadt, B. Stengel, and B. M. Thompson, *Microwave Differential Circuit Design Using Mixed-Mode S-Parameters*. Norwood, MA, USA: Artech House, 2006.
[39] T. H. Bui, H. T. Vu, S. X. Ta, K. K. Nguyen, C. Dao-Ngoc, and N. Nguyen-Trong, "Dual-band dual-polarized slotted-patch antenna for in-band full-duplex applications," *IEEE Antennas Wireless Propag. Lett.*, vol. 22, pp. 1286–1290, 2023.
[40] J. Liu, Q. Xue, H. Wong, H. W. Lai, and Y. Long, "Design and analysis of a low-profile and broadband microstrip monopolar patch antenna," *IEEE Trans. Antennas Propag.*, vol. 61, no. 1, pp. 11–18, Jan. 2013.
[41] Z.-Y. Zhang, Y.-X. Guo, L. C. Ong, and M. Chia, "A new wide-band planar balun on a single-layer PCB," *IEEE Microw. Wireless Compon. Lett.*, vol. 15, no. 6, pp. 416–418, Jun. 2005.
[42] B. Schiek and J. Kohler, "A method for broad-band matching of microstrip differential phase shifters," *IEEE Trans. Microw. Theory Tech.*, vol. 25, no. 8, pp. 666–671, Aug. 1977.

SON XUAT TA (Senior Member, IEEE) received the B.Sc. (Eng.) degree in electronics and telecommunications from the Hanoi University of Science and Technology, Vietnam, in August 2008, and the Ph.D. degree in electrical engineering from Ajou University, South Korea, in February 2016. From March 2016 to February 2017, he was a Postdoctoral Research Fellow with the Department of Electrical and Computer Engineering, Ajou University. From March 2017 to August 2017, he was with Ton Duc Thang University, Ho Chi Minh City, Vietnam. Since September 2017, he has been working as a Lecturer with the School of Electrical and Electronic Engineering, Hanoi University of Science and Technology. He has authored and coauthored over 100 technical journal and conference papers. His research interests include antennas, metamaterials, metasurfaces, metamaterial-based antennas, metasurface-inspired antennas, circularly polarized antennas, and millimeter-wave antennas. He was selected as a Top Reviewer for IEEE TRANSACTIONS ON ANTENNAS AND PROPAGATION in 2020–2023. He has served as a reviewer for over 20 scientific journals.

TRAN HIEN BUI received the B.Sc. (Eng.) degree in electronics and telecommunication engineering from the Hanoi University of Science and Technology, Vietnam, in 2023, where he worked as an Internship Researcher with the Communication Research and Development Laboratory from May 2020 to December 2023. His research interests include diversity antennas, multipolarized antennas, and multiband antennas.

KHAC KIEM NGUYEN (Member, IEEE) was born in Hanoi, Vietnam, in 1978. He received the B.Eng., M.Sc., and Ph.D. degrees from the School of Electrical and Electronic Engineering (SEEE), Hanoi University of Science and Technology (HUST), Vietnam, in 2001, 2003, and 2017, respectively. Since 2001, he has been working as a Lecturer with SEEE, HUST and a Researcher with CRD LAB, HUST. His research interests include design microstrip antenna for next-generation mobile communication systems as well as passive RF components.

NGHIA NGUYEN-TRONG (Senior Member, IEEE) received the Ph.D. degree (Doctoral Research Medal) in electrical engineering from The University of Adelaide, Adelaide, SA, Australia, in 2017.

He is currently with Nextwaves Industries. His main research interests include microwave circuits, advanced materials, absorbers, and various types of antennas.

Dr. Nguyen-Trong was one of the recipients of the Best Student Paper Award at the 2014 IWAT, the 2015 IEEE MTT-S NEMO, and the 2017 ASA Conferences, and the Best Paper Award at the 2018 and 2020 AMS Conference. He has been continuously selected as a Top Reviewer for IEEE TRANSACTIONS ON ANTENNAS AND PROPAGATION in 2018–2021 and IEEE ANTENNA WIRELESS AND PROPAGATION LETTERS in 2018 and 2021. He serves as a Technical Co-Chair for the 2020 Australian Microwave Symposium and the 2022 IEEE International Symposium on Antennas and Propagation. He is listed among Australia's Top 40 Early Career Researchers by The Australian, November 2021.